NASA Technical Paper 3418

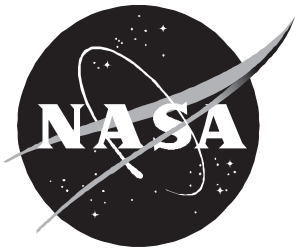

Design and Evaluation of an Electromagnetic Beam Waveguide for Measuring Electrical Properties of Materials

M. C. Bailey

February 1994

NASA Technical Paper 3418

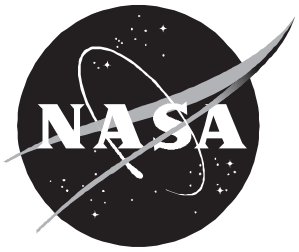

Design and Evaluation of an Electromagnetic Beam Waveguide for Measuring Electrical Properties of Materials

M. C. Bailey
Langley Research Center • Hampton, Virginia

National Aeronautics and Space Administration
Langley Research Center • Hampton, Virginia 23681-0001

February 1994

National Aeronautics and
Space Administration
Code JTT
Washington, D.C.
20546-0001

Official Business
Penalty for Private Use, $300

B U L K R A T E
POSTAGE & FEES PAID
NASA Permit No. G-27

Postmaster: If undeliverable (Section 158 Postal Manual) Do Not Return

Abstract

A beam waveguide has been designed that is based upon the propagation characteristics of the fundamental Gaussian beam and the focusing properties of spherical dielectric lenses. The 20-GHz, two-horn, four-lens system was constructed and experimentally evaluated by probing the field in a plane perpendicular to the beam axis at the center of the beam waveguide system. The critical parameters were determined by numerical sensitivity studies, and the lens-horn critical spacing was adjusted to better focus the beam at the probe plane. The measured performance was analyzed by consideration of higher order Gaussian-Laguerre beam modes. The beam waveguide system was successfully used in the measurements of the electromagnetic transmission properties of Shuttle thermal-protection tiles while the tile surface was being heated to reentry-level temperatures with a high-power laser.

Introduction

In the determination of the electrical characteristics of materials, measuring the magnitude and phase of the plane wave reflection and transmission coefficients of the material at the frequency of interest is often desirable. Interpretation of the electrical properties from these measurements is greatly simplified by using a planar sheet of the material; however, difficulties are sometimes encountered in producing a plane wave through a sheet of material of very limited surface area. One approach is to place a precision-machined sample of the material in a metal-enclosed cavity or waveguide; however, cutting the material to obtain a sample destroys the original sheet. Another approach is to transmit and receive plane waves with a horn antenna on each side of the sheet. In the two-horn approach, diffractions from the edges of the sheet can cause significant errors in the measurements. The present approach uses small horns and a series of quartz lenses to focus the electromagnetic field on the surface of the sheet of test material, at some distance from each horn aperture, to a small circular cross section and uniform phase.

The motivation for the present design was the need for measurement of the electrical characteristics of Shuttle thermal-protection tile when the outer surface of the tile is heated to very high temperatures, such as those encountered during atmospheric reentry. The technique chosen for heating the tile surface was to utilize a high-output laser directed toward one side of the tile. The heating of the tile surface could be controlled by the laser beam diameter and laser output power. The laser beam diameter was adjusted to approximately 4 in. and was directed toward the tile surface at an incidence angle of approximately 40°. This laser system allowed essentially uniform heating of the 4-in. central portion of a 6- by 6-in. sample of tile material. A detailed description of the experiment is contained in reference 1. The present report describes the design of the 20-GHz beam waveguide system used in that experiment for transmission measurements.

The design objective was to transmit an electromagnetic wave with a planar phase front and more than 90 percent of the power contained within the heated portion of the tile surface. Because of the requirement of an unblocked line of sight for the laser heating, all components of the 20-GHz system were placed at some distance from the tile while producing an electromagnetic wave at normal incidence to the tile surface. The technique for achieving the objective is illustrated in figure 1. The 20-GHz system consists of two small horns and four quartz focusing lenses in a Gaussian beam waveguide. The pertinent equations for Gaussian beam propagation and the focusing properties of spherical lenses are reviewed in the next two sections. In later

sections, the fundamental Gaussian beam mode is used for the design and sensitivity studies of the present beam waveguide system and measured results are presented for evaluation.

Symbols

$A_{\alpha n}$	amplitude of (α, n) Gaussian-Laguerre beam mode
a	radius of horn aperture
D	diameter of lens
d_1	distance from input beam waist to entrance principal plane of first lens
d_2	distance from exit beam waist to exit principal plane of first lens
d_3	distance from entrance beam waist to entrance principal plane of second lens
d_4	distance from exit beam waist to exit principal plane of second lens
e	base of natural system of logarithms ($e = 2.718281828459$)
F_1	focal length of first lens
F_2	focal length of second lens
$J_0(\ )$	Bessel function of first kind of order 0
j	$= \sqrt{-1}$
k	free-space propagation constant, $2\pi/\lambda$
L_1	distance from entrance beam waist to center of first lens in beam waveguide
L_2	center-to-center axial spacing between first and second lenses in beam waveguide
L_3	distance along axis from center of second lens to center of beam waveguide
$L_n^{(\alpha)}$	generalized Laguerre polynomial
n	index of radial variation in beam field distribution
R	radius of curvature of beam phase front
R_1	radius of curvature of lens nearest to horn (i.e., first lens)
R_2	radius of curvature of lens farthest from horn (i.e., second lens)
r	radius of curvature of lens entrance surface
r'	radius of curvature of lens exit surface
rms	root mean square
T	thickness of lens
T_1	edge thickness of lens nearest to horn
T_2	edge thickness of lens farthest from horn
u	principal plane at entrance side of lens
u'	principal plane at exit side of lens
w	half-width of beam (where field equals e^{-1} of on-axis value)
w_0	half-width of beam at beam waist
w_1	half-width of beam at entrance beam waist of first lens

w_2	half-width of beam at exit beam waist of first lens and entrance beam waist of second lens
w_3	half-width of beam at exit beam waist of second lens
x, y	rectangular coordinates
z	cylindrical coordinate variable along axis of beam in direction of propagation
z'	axial distance from exit beam waist of second lens to probe plane
z_0	axial distance from entrance Gaussian beam waist to horn aperture
α	index of circumferential variation in beam field distribution
γ	quadratic phase taper across width of beam
Δ	quantity defined by equation (13)
δ	axial distance between lens entrance surface and lens entrance principal plane
δ'	axial distance between lens exit surface and lens exit principal plane
ε_0	permittivity of vacuum
ε_1	permittivity of dielectric lens
ε_r	relative dielectric constant of lens, $\varepsilon_1/\varepsilon_0$
λ	wavelength of field
ξ_1	spacing between principal planes for first lens
ξ_2	spacing between principal planes for second lens
ρ	cylindrical coordinate variable in radial direction
σ	reciprocal of standard deviation for Gaussian distribution
Φ_{00}	propagation phase delay of fundamental Gaussian beam mode
$\Phi_{\alpha n}$	propagation phase delay of (α, n) Gaussian-Laguerre beam mode
ϕ	cylindrical coordinate variable in circumferential direction
χ	argument of Laguerre polynomial
ψ	scalar field quantity

Gaussian Beam Characteristics

Since the late 1950's Gaussian beam theory has been extensively utilized in laser systems. A good basic review of the theory of laser beams and resonators is contained in reference 2. The concept of electromagnetic wave beams was also introduced in the early 1960's (ref. 3) and was utilized in a millimeter wave beam waveguide with phase-correcting lenses (ref. 4).

For a wave propagating in the z-direction, an approximate solution (ref. 2) to the wave equation, valid near the axis of propagation, can be rewritten in cylindrical coordinates as

$$\psi(\rho,\phi,z) = \left[\frac{w_0}{w(z)}\right] \exp\left[-\left(\frac{\rho}{w(z)}\right)^2\right] \exp\left[-j\left(\frac{k\rho^2}{2\,R(z)}\right)\right] \exp(-jkz)$$
$$\times \sum_{n=0}^{\infty}\sum_{\alpha=0}^{\infty} A_{\alpha n}\left[\sqrt{2}\frac{\rho}{w(z)}\right]^{\alpha} L_n^{(\alpha)}\left\{2\left[\frac{\rho}{w(z)}\right]^2\right\}$$
$$\times \exp(-j\alpha\phi)\ \exp\left[j\,(2n+\alpha+1)\ \tan^{-1}\left(\frac{\lambda z}{\pi w_0^2}\right)\right] \qquad (1)$$

The function $L_n^{(\alpha)}(\chi)$ in equation (1) denotes the generalized Laguerre polynomials and can be calculated from Rodriques' formula

$$L_n^{(\alpha)}(\chi) = \left(\frac{1}{n!\chi^\alpha e^{-\chi}}\right)\frac{d^n}{d\chi^n}\left(\chi^{n+\alpha}e^{-\chi}\right) \tag{2}$$

(ref. 5, p. 785), where the operator $d^0/d\chi^0$ is defined as unity.

Use of equation (2) for $n = 0$ and $n = 1$ yields

$$\left.\begin{aligned} L_0^{(\alpha)}(\chi) &= 1 \\ L_1^{(\alpha)}(\chi) &= \alpha + 1 - \chi \end{aligned}\right\} \tag{3}$$

Equation (2) is valid for polynomials of all degrees; however, the recurrence relations with respect to degree n given by

$$(n+1)\,L_{n+1}^{(\alpha)}(\chi) = (2n + \alpha + 1 - \chi)\,L_n^{(\alpha)}(\chi) - (n+\alpha)\,L_{n-1}^{(\alpha)}(\chi) \tag{4}$$

(ref. 5, p. 782) can be used to more readily obtain the polynomials of degree $n > 1$.

In equation (1) the indices n and α represent the cross-sectional modal variations for the beam field distribution in the radial and circumferential directions, respectively. The fundamental mode field ($\alpha = 0$, $n = 0$) reduces to

$$\psi(\rho,\phi,z)\Big|_{\substack{\alpha=0\\ n=0}} = A_{00}\left[\frac{w_0}{w(z)}\right]\exp\left\{-\left[\frac{\rho}{w(z)}\right]^2\right\}\exp(-jkz)$$

$$\times\exp\left\{-j\left[\frac{k\rho^2}{2\,R(z)}\right]\right\}\exp\left[j\ \tan^{-1}\left(\frac{\lambda z}{\pi w_0^2}\right)\right] \tag{5}$$

and exhibits the Gaussian amplitude distribution ($\exp(-\sigma\rho^2)$) with a quadratic phase distribution ($\exp(-j\gamma\rho^2)$). Higher order modes are referred to as "Gaussian-Laguerre modes."

In addition to the mode indices, two other parameters characterize the beam cross-sectional distribution. These parameters are the radius of curvature of the beam phase front and the half-width of the beam (defined as the radial distance where the field has decreased to e^{-1} of the value on axis). These parameters are a function of the distance along the axis of the beam and are presented, respectively, as

$$R(z) = z\left[1 + \left(\frac{\pi w_0^2}{\lambda z}\right)^2\right] \tag{6}$$

and

$$w(z) = w_0\left[1 + \left(\frac{\lambda z}{\pi w_0^2}\right)^2\right]^{1/2} \tag{7}$$

At the beam waist where $w(0) = w_0$ and $R(0) = \infty$, the beam has its smallest cross section and the phase front is planar.

Figure 2 illustrates the spreading of the beam for the fundamental Gaussian mode as a function of the distance from the beam waist along the beam axis. Figure 3 shows a plot of the

beam diameter ($2w$), radius of curvature of the phase front (R), and the beam quadratic phase taper (γ) as a function of the distance (z) from the beam waist at a frequency of 20 GHz and beam waist diameter of 2 in. The beam spot size of 2 in. is chosen as the objective of the system design for measurements of tile properties (ref. 1).

Beam Transformation by a Lens

When a Gaussian beam with a waist diameter of $2w_1$ passes through a lens, the parameters in the beam expansion laws (ref. 6) are changed and a new Gaussian beam with a waist diameter of $2w_2$ is formed on the other side of the lens. The beam waist diameters are related by

$$w_2^2 = w_1^2 \left[\frac{F_1^2}{(d_1 - F_1)^2 + (\pi w_1^2/\lambda)^2} \right] \tag{8}$$

(ref. 6) where F_1 is the focal length of the lens and the distances d_1 and d_2 to the beam waists are related by (ref. 6)

$$(d_2 - F_1) = (d_1 - F_1) \left[\frac{F_1^2}{(d_1 - F_1)^2 + (\pi w_1^2/\lambda)^2} \right] \tag{9}$$

Equations (8) and (9) were developed for an ideal thin lens; however, these results are applicable also to a thick lens if d_1 and d_2 are interpreted as the distances from the beam waists to the principal planes of the thick lens. By referring to figure 4, the focal length and locations of the principal planes u and u' can be determined for the thick lens as

$$F_1 = \sqrt{\varepsilon_r}\, \frac{rr'}{\Delta} \tag{10}$$

$$\delta = (\sqrt{\varepsilon_r} - 1)\, \frac{rT}{\Delta} \tag{11}$$

$$\delta' = (\sqrt{\varepsilon_r} - 1)\, \frac{r'T}{\Delta} \tag{12}$$

(ref. 7) where

$$\Delta = (\sqrt{\varepsilon_r} - 1) \left[\sqrt{\varepsilon_r}\, (r + r') - T (\sqrt{\varepsilon_r} - 1) \right] \tag{13}$$

with T being the total (on axis) thickness of the lens.

Figure 5 illustrates Gaussian beam transformation through thick convex-convex and plano-convex lenses. Symmetrical ($r = r'$) convex-convex quartz lenses ($\varepsilon_r = 3.78$) are used in the present beam waveguide design.

For the special case of a Gaussian beam launched at the focal plane of a lens ($d_1 = F_1$), equation (9) yields

$$d_1 = d_2 = F_1 \tag{14}$$

and equation (8) yields

$$w_2 = \frac{\lambda F_1}{\pi w_1} \tag{15}$$

Equations (14) and (15) are used in the design of the beam waveguide described in the next section; however, in the sensitivity studies in a later section, equations (8) and (9) are used for the calculations. Numerical studies have shown that selection of the lens focal plane as the entrance beam waist location provides the least sensitive condition with respect to parameter variations.

Beam Waveguide Design

The objective of the beam waveguide design is to transmit a wave that produces a spot approximately 2 in. in diameter with a uniform phase front at the surface of the material that is being tested for its transmission characteristics. The allowance of an unblocked laser beam for heating the surface of the tile under test is also required.

The geometry of the system is illustrated in figure 1. A parametric study was used to determine the lens dimensions and spacings that would be practical to implement. The final design dimensions are illustrated in figure 6 for one-half of the beam waveguide system. The beam waveguide is symmetrical about the spot focusing plane, where $2w_3 = 2.0$ in.

Because equation (15) applies to any lens, a similar expression can be obtained for the second lens in the system, which is given as

$$w_3 = \frac{\lambda F_2}{\pi w_2} \tag{16}$$

In the design of the two-lens system, the exit beam waist for the first lens is also the entrance beam waist for the second lens; therefore, combining equations (15) and (16) yields

$$\frac{w_3}{w_1} = \frac{F_2}{F_1} \tag{17}$$

for the relationship between the entrance and exit beam waist spot sizes, as shown in figure 6. Note that the ratio of the entrance and exit beam waist diameters is determined only by the ratio of the focal lengths of the two lenses; however, equation (17) assumes fundamental mode propagation and location of entrance beam waist at the focal plane of the first lens.

Figure 7 shows a plot of the beam diameter and phase taper as a function of the distance along the axis of the beam. Notice that this design provides a well-focused beam over a significant axial distance, thus allowing a reasonable test zone for materials.

A numerical sensitivity study was conducted to determine which parameters of the design in figure 6 are the most critical. The quantities of interest in the sensitivity study were the beam diameter and phase taper at the test zone (i.e., the symmetric plane of the beam waveguide system). Figures 8–12 show the variation of these quantities with changes in the design parameters. These calculations were obtained by repetitive application of equations (6)–(9) with the value of $2w_1 = 0.66$ in. at the entrance beam waist on the left side of the beam waveguide. The results in figures 8 and 9 indicate that the primary effect of inaccuracies in the design parameters is to shift the beam spot in the axial direction. Figures 10–12 show the variation in the beam diameter and phase taper at the center of the test zone versus changes in the lens parameters. From the data of figures 8–12, the most critical parameter appears to be the spacing (L_1) between the launching plane for the entrance beam waist and the first lens. Earlier experimental studies (ref. 4) reached similar conclusions for the spacing between the launcher and the first lens. Also, an accurate determination of the equivalent location of the beam waist for a microwave horn is difficult. For these reasons, the physical setup of the system was configured to allow a micrometer adjustment of the spacing between the horn and the first lens.

In order to produce a circular spot beam, the utilization of a horn antenna that radiates a circularly symmetric beam is highly desirable. A dual-mode conical horn (ref. 8) would satisfy this requirement. The horn should be designed to launch a fundamental Gaussian beam with an equivalent beam waist diameter of 0.66 in. at 20 GHz. The ratio of the beam waist diameter to the horn aperture diameter for a corrugated conical horn can be calculated as

$$\frac{2w_0}{2a} = 0.6435 \tag{18}$$

(ref. 9) where a is the radius of the horn aperture. Because the radiation patterns of dual-mode conical horns and corrugated conical horns are very similar, equation (18) should also be applicable to dual-mode conical horns as well. Thus, for a beam waist diameter of 0.66 in., equation (17) indicates that a horn aperture diameter of 1.03 in. would be required. Based upon the equations of reference 8, dual-mode horns were designed and fabricated for the beam waveguide system, with the internal dimensions shown in figure 13.

The remaining design parameter to be determined was the location of the equivalent Gaussian beam waist relative to the horn physical aperture. This was accomplished by matching the radius of curvature for the Gaussian beam to the aperture quadratic phase taper of the conical horn. The distance from the beam waist where this match occurs ($z_0 = 0.06$ in.) was taken to be the distance inside the conical horn where the Gaussian beam is launched, as illustrated in figure 14. This procedure could also be used as a means of locating the far-field phase center for conical horns. Because this procedure, in conjunction with equation (17), is an estimate, the allowance for adjustment capability for spacing between the horn and first lens in the physical setup is highly desirable.

Measured Results

The beam waveguide design was experimentally evaluated by probing the electric field in the symmetric plane across the beam. Both amplitude (in decibels) and phase (in degrees) were recorded in a raster scan. After the field was probed for the initial setup according to the designed spacing of the horns and lenses, the distance between the horns and lenses on each end was adjusted in an attempt to focus the beam better in the probed plane (i.e., produce a more uniform phase). Contour plots of the measured amplitude before and after adjustment are shown in figures 15 and 16, respectively. The beam is obviously focused into a smaller spot after the adjustment. The adjustment resulted in a shortening of the horn-lens spacing by 0.291 in. The amplitudes in the H-plane ($x = 0$) and E-plane ($y = 0$) are plotted in figures 17 and 18, respectively, along with a Gaussian beam shape with the same beamwidth at the e^{-1} level (-8.686 dB) in each case. The corresponding H-plane and E-plane phase plots are given in figures 19 and 20, respectively. The smooth solid curves are an average of the measured data points. One can readily note that the phase is more uniform over the beamwidth after the adjustment and that the beamwidth, in addition to becoming smaller, is also more circular after adjustment. A further adjustment in spacing was not attempted because the results were determined to be adequate for the intended transmission tests of the heated tiles.

Higher Order Modes

The design of the beam waveguide system was based upon the assumption that only the fundamental Gaussian mode was launched by the horn and that a pure first-order Gaussian beam propagated throughout the lens focusing system. A more accurate model of the beam waveguide system can be obtained by considering the higher order Gaussian-Laguerre modes. The launching coefficients of higher order modes can be obtained by matching the aperture fields for a corrugated conical horn (ref. 9). These coefficients are listed in table I. Also listed in table I are modal coefficients obtained by performing a least-squared fit of the first 11 circularly symmetric (i.e., α independent) modes to the function $J_0(2.405\rho/a)$, which is the aperture field distribution of a corrugated conical horn with no phase taper. The aperture distributions using the modal coefficients of table I are compared in figure 21 with the function $J_0(2.405\rho/a)$. The distribution with the least-squared-fit coefficients results in a better approximation to the aperture field function.

The cross-sectional distribution is calculated from equation (1) at the beam waist ($z = 0$) and includes the higher order modes in table I. These calculations are compared in figure 22

with the fundamental mode distribution. Inclusion of the higher order modes results in a slight broadening of the beamwidth (at the −8.686-dB level) and in the appearance of side lobes. These observations were also evident in the measured data and indicate that higher order modes should be considered in future designs. Also, as noted in figure 22, the least-squared-fit modal coefficients appear to yield side lobe levels corresponding more closely with those observed in the measured data of figures 17 and 18 after the experimental system was adjusted.

By use of equation (1), the differential change in phase of the higher order modes (relative to the fundamental mode) propagating in the z-direction is given by

$$(\Phi_{\alpha n} - \Phi_{00}) = (2n + \alpha)\,\Phi_{00} \tag{19}$$

where the phase delay of the propagating fundamental mode is given by

$$\Phi_{00} = \tan^{-1}\left(\frac{\lambda z}{\pi w_0^2}\right) \tag{20}$$

When equation (20) is applied consecutively to each section of the beam waveguide, the total phase delay for the fundamental mode that propagates from the entrance of the beam waveguide to the probe plane becomes

$$\Phi_{00} = \tan^{-1}\left(\frac{\lambda d_1}{\pi w_1^2}\right) + \tan^{-1}\left(\frac{\lambda d_2}{\pi w_2^2}\right) + \tan^{-1}\left(\frac{\lambda d_3}{\pi w_2^2}\right) + \tan^{-1}\left(\frac{\lambda d_4}{\pi w_3^2}\right) + \tan^{-1}\left(\frac{\lambda z'}{\pi w_3^2}\right) \tag{21}$$

where z' is the distance of the probe plane past the exit beam waist. The quantities in equation (21) are related to the parameters in figure 6 by

$$d_1 = \left(L_1 - \frac{1}{2}\xi_1\right)$$

$$d_3 = \left[L_2 - d_2 - \frac{1}{2}\left(\xi_1 + \xi_2\right)\right]$$

$$z' = \left(L_3 - d_4 - \frac{1}{2}\xi_2\right)$$

The values of ξ_1 and ξ_2 are the spacings between principal planes (u and u') for the first and second lenses, respectively. (That is, $\xi_1 = 1.071$ in. and $\xi_2 = 0.416$ in.) The other quantities in equation (21) can be related by applying equations (8) and (9); thus,

$$d_2 = F_1 + \frac{(d_1 - F_1)\,F_1^2}{(d_1 - F_1)^2 + \left(\pi w_1^2/\lambda\right)^2}$$

$$d_4 = F_2 + \frac{(d_3 - F_2)\,F_2^2}{(d_3 - F_2)^2 + \left(\pi w_2^2/\lambda\right)^2}$$

$$w_2^2 = w_1^2\left[\frac{F_1^2}{(d_1 - F_1)^2 + \left(\pi w_1^2/\lambda\right)^2}\right]$$

$$w_3^2 = w_2^2\left[\frac{F_2^2}{(d_3 - F_2)^2 + \left(\pi w_2^2/\lambda\right)^2}\right]$$

For the special case of $z' = 0$, $d_1 = d_2 = F_1$, and $d_3 = d_4 = F_2$, equation (21) can be written as

$$\Phi_{00} = \tan^{-1}\left(\frac{\lambda F_1}{\pi w_1^2}\right) + \tan^{-1}\left[\frac{\lambda F_1}{\pi w_1^2}\left(\frac{F_1}{F_2}\right)\right] + \tan^{-1}\left(\frac{\pi w_1^2}{\lambda F_1}\right) + \tan^{-1}\left[\frac{\pi w_1^2}{\lambda F_1}\left(\frac{F_2}{F_1}\right)\right] \qquad (22)$$

Equation (22) yields a value of $\Phi_{00} = \pi$ for the geometry of figure 6. Because losses in the system are neglected and the higher order modes experience a differential phase shift of $2n\pi$, the mode amplitudes in table I also apply to the output of the beam waveguide system.

Figure 23 shows calculations of the cross-sectional distribution of the beam including the effects due to the higher order modes with various amounts of phase delay for the system of figure 6. The phase delay variations could be caused by several factors, such as lack of accurate knowledge of the entrance beam waist location, inaccuracies in the system parameters, and unknown modal field structures and phase delays internal to the lenses. Figure 23 shows that in addition to a nonuniform phase distribution, the most significant effect of phase delay (or modal phase slippage) is a fill-in between the nulls of the side lobes. This null fill-in was also observed in the measured data.

Concluding Remarks

A beam waveguide system consisting of two dual-mode horns and four lenses has been designed for spot focusing of a 20-GHz electromagnetic wave beam onto a sheet of dielectric material. The design was accomplished by using fundamental-mode Gaussian beam propagation properties. Experimental tests, in conjunction with analytical calculations, indicate the presence of higher order Gaussian-Laguerre modes in the system. However, the experimental system, designed by using only the fundamental mode, was considered to be sufficient for measuring the plane-wave propagation characteristics of the dielectric sheet under test.

NASA Langley Research Center
Hampton, VA 23681-0001
January 4, 1994

References

1. Heil, Garrett G.: *High Temperature Electromagnetic Characterization of Thermal Protection System Tile Materials.* NASA CR-189687, 1993.

2. Kogelnik, H.; and Li, T.: Laser Beams and Resonators. *Proc. IEEE*, vol. 54, no. 10, Oct. 1966, pp. 1312–1329.

3. Goubau, G.; and Schwering, F.: On the Guided Propagation of Electromagnetic Wave Beams. *IRE Trans. Antennas & Propag.*, vol. AP-9, May 1961, pp. 248–256.

4. Christian, J. R.; and Goubau, G.: Experimental Studies on a Beam Waveguide for Millimeter Waves. *IRE Trans. Antennas & Propag.*, vol. AP-9, May 1961, pp. 256–263.

5. Abramowitz, Milton; and Stegun, Irene A., eds.: *Handbook of Mathematical Functions.* Dover Publ., Inc., 1965.

6. Kogelnik, Herwig: Imaging of Optical Modes—Resonators With Internal Lenses. *Bell Syst. Tech. J.*, vol. 4, Mar. 1965, pp. 455–494.

7. Born, Max; and Wolf, Emil: *Principles of Optics, Second revised ed.* Macmillan Co., 1964.

8. Potter, P. D.: A New Horn Antenna With Suppressed Sidelobes and Equal Beamwidths. *Microw. J.*, vol. 6, June 1963, pp. 71–78. (Available as NASA CR-50625.)

9. Wylde, R. J.: Millimetre-Wave Gaussian Beam-Mode Optics and Corrugated Feed Horns. *IEE Proc.*, vol. 131, pt. H, no. 4, Aug. 1984, pp. 258–262.

Table I. Complex Coefficients for Gaussian-Laguerre Beam-Mode Expansion of Aperture Fields for Corrugated Horn

n	A_{0n}/A_{00} coefficients from—	
	Reference 9	Present study
0	$1 + j0$	$1 + j0$
1	$-0.00007 + j0$	$0.00142 - j0.00118$
2	$-0.12177 + j0$	$-0.12369 - j0.00072$
3	$-0.04358 + j0$	$-0.06234 + j0.00179$
4	$0.01972 + j0$	$0.02621 + j0.00090$
5	$0.03441 + j0$	$0.06749 - j0.00292$
6	$0.02015 + j0$	$0.03022 - j0.00173$
7	$0.00012 + j0$	$-0.03769 - j0.00111$
8	$-0.01272 + j0$	$-0.04492 + j0.00059$
9	$-0.01542 + j0$	$-0.01840 + j0.00250$
10	$-0.01070 + j0$	$0.04702 - j0.00120$

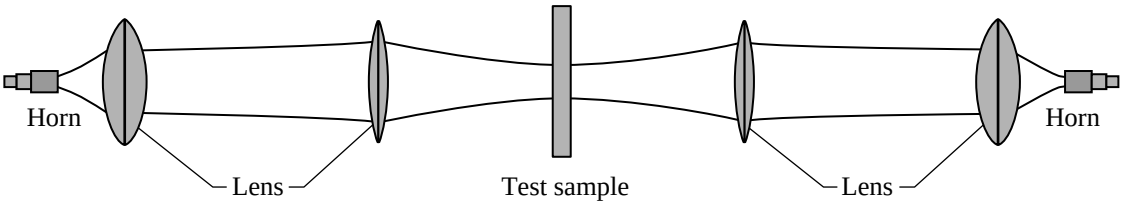

Figure 1. Beam waveguide system for measuring transmission characteristics of planar dielectric sheet.

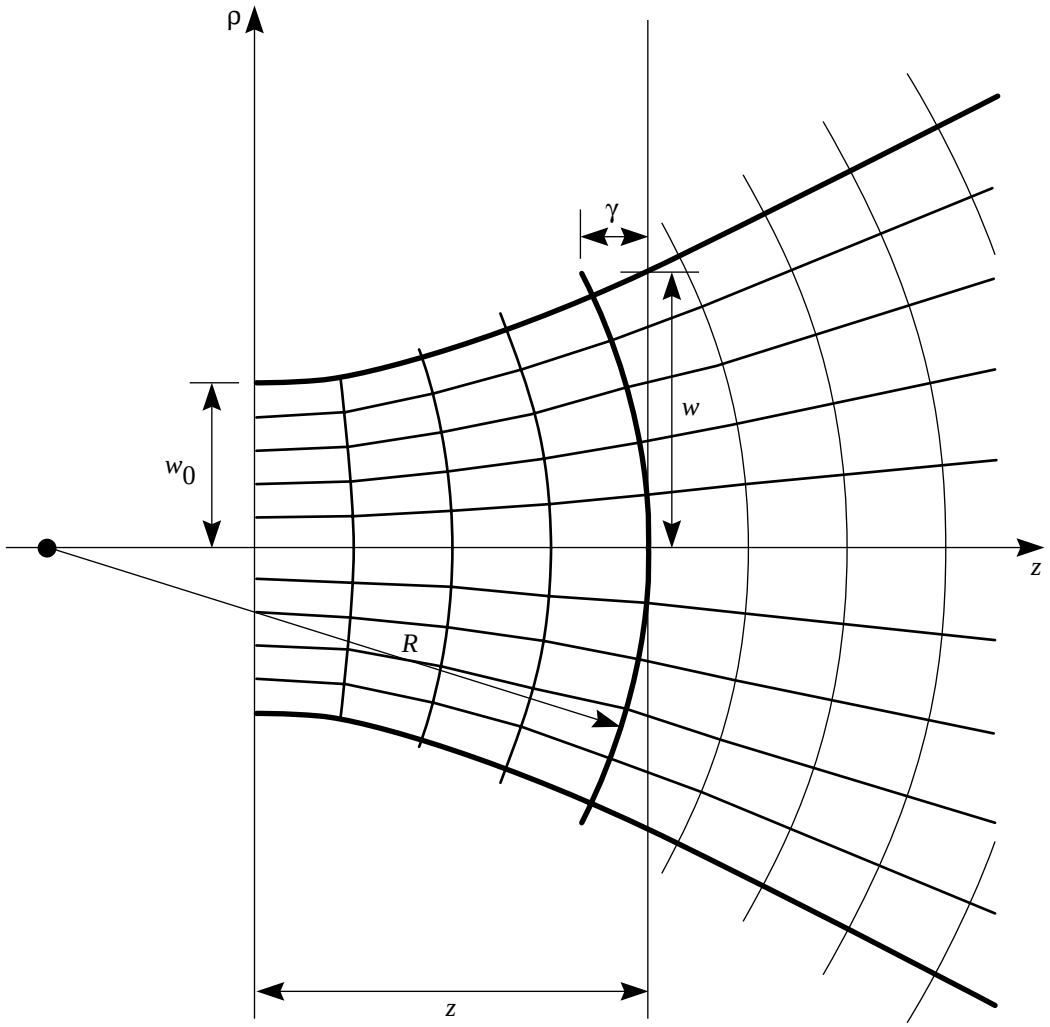

Figure 2. Geometry of propagating Gaussian beam.

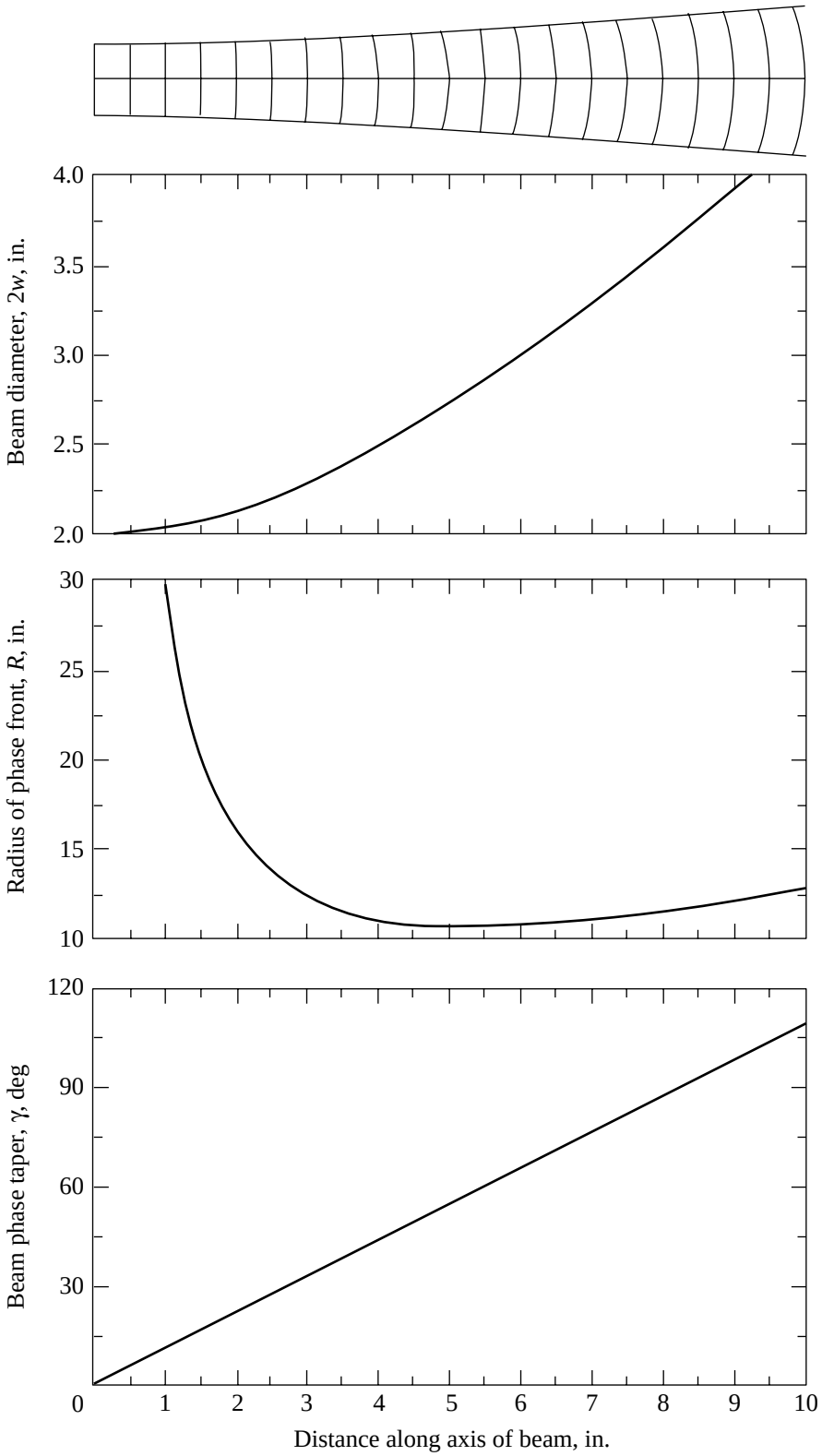

Figure 3. Gaussian beam characteristics versus distance along axis of propagation.

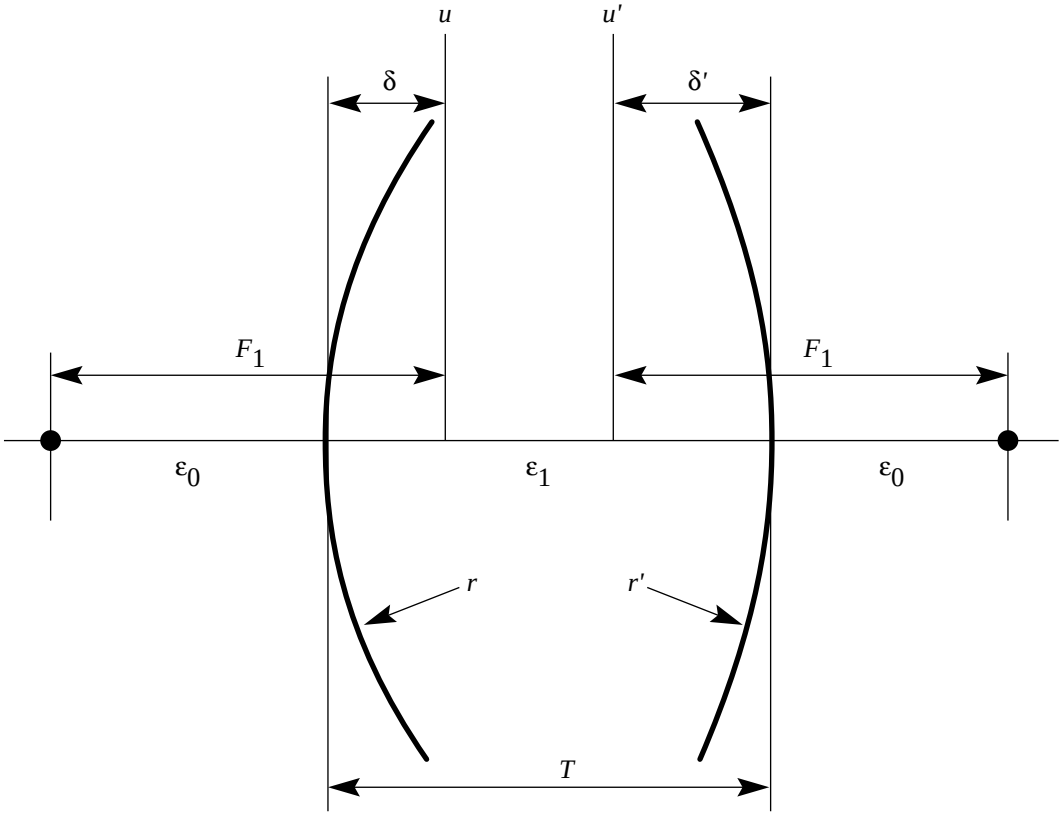

Figure 4. Parameters for thick dielectric lens with spherical surfaces at entrance and exit surfaces.

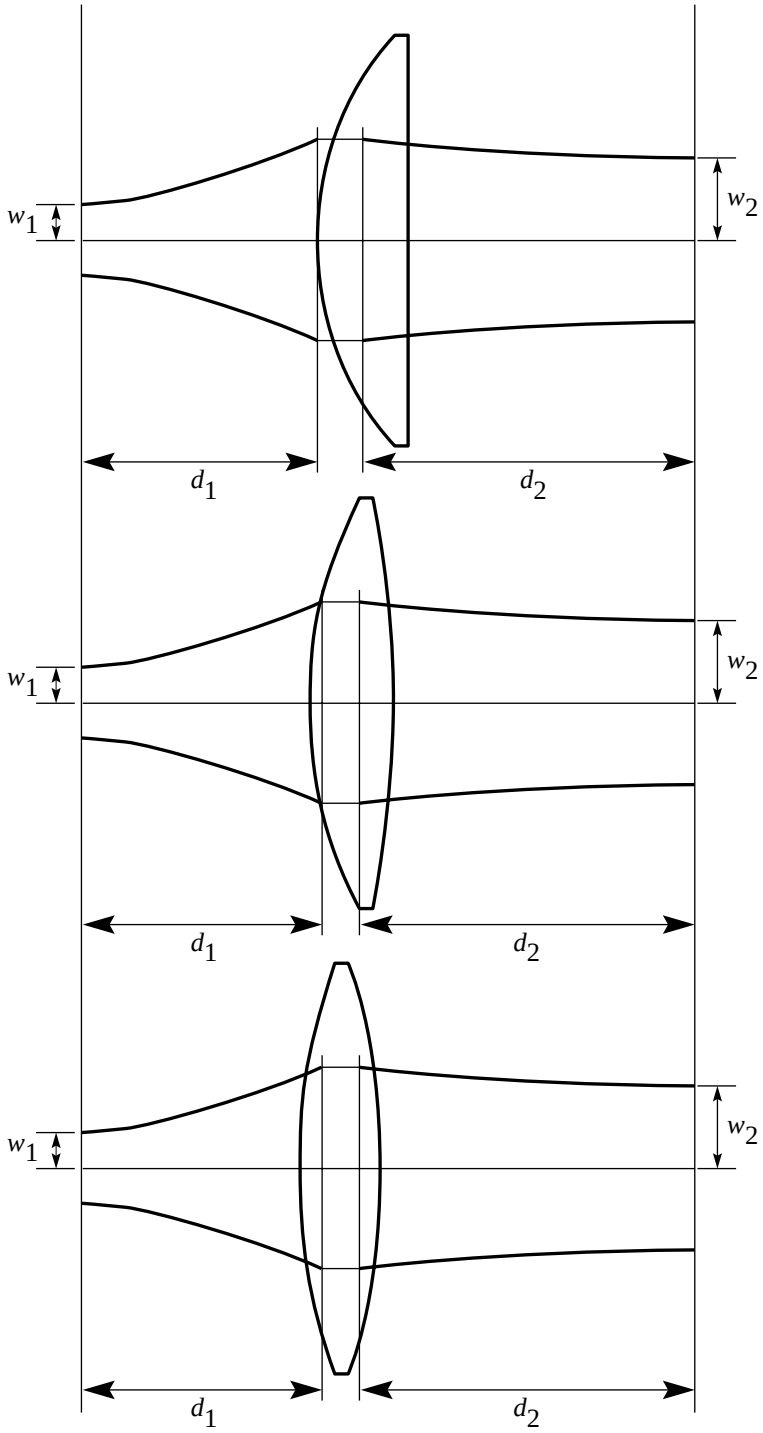

Figure 5. Gaussian beam transformation with thick dielectric lenses.

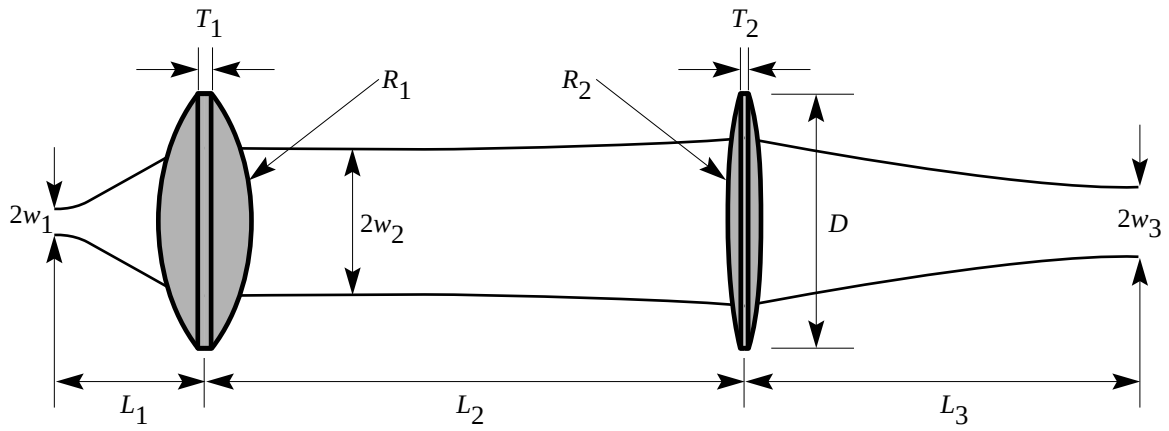

$L_1 = 4.071$	$2w_1 = 0.66$	$R_1 = 6.0$	$T_1 = 0.25$
$L_2 = 14.983$	$2w_2 = 4.03$	$R_2 = 20.0$	$T_2 = 0.25$
$L_3 = 10.912$	$2w_3 = 2.00$	$D = 7.0$	$\varepsilon_r = 3.78$

Figure 6. Design parameters for spot-focusing beam waveguide system. All dimensions are given in inches.

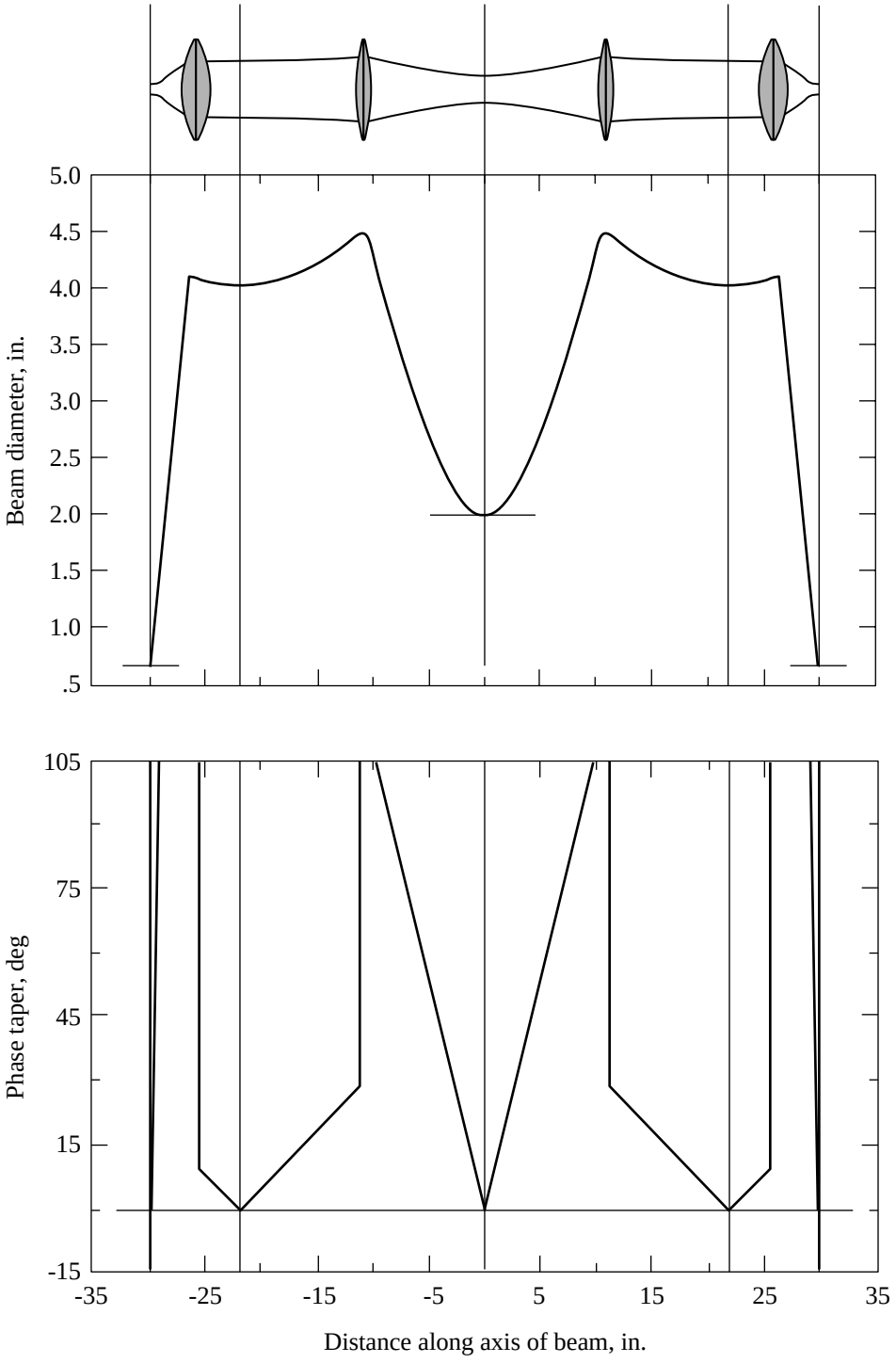

Figure 7. Beam characteristics for 20-GHz beam waveguide system.

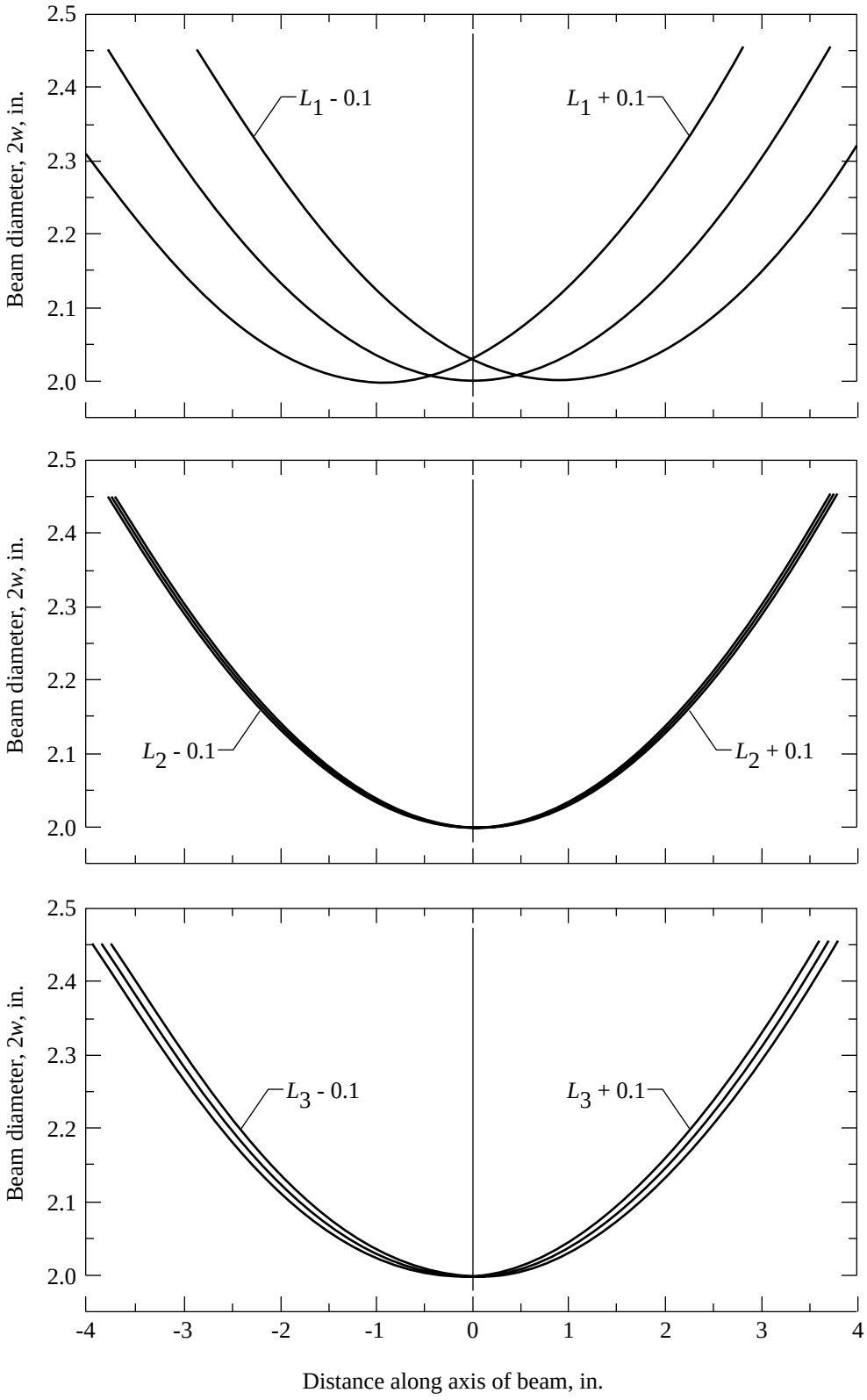

Figure 8. Beam diameter characteristics in test region versus sensitivity to axial errors in 20-GHz beam waveguide system.

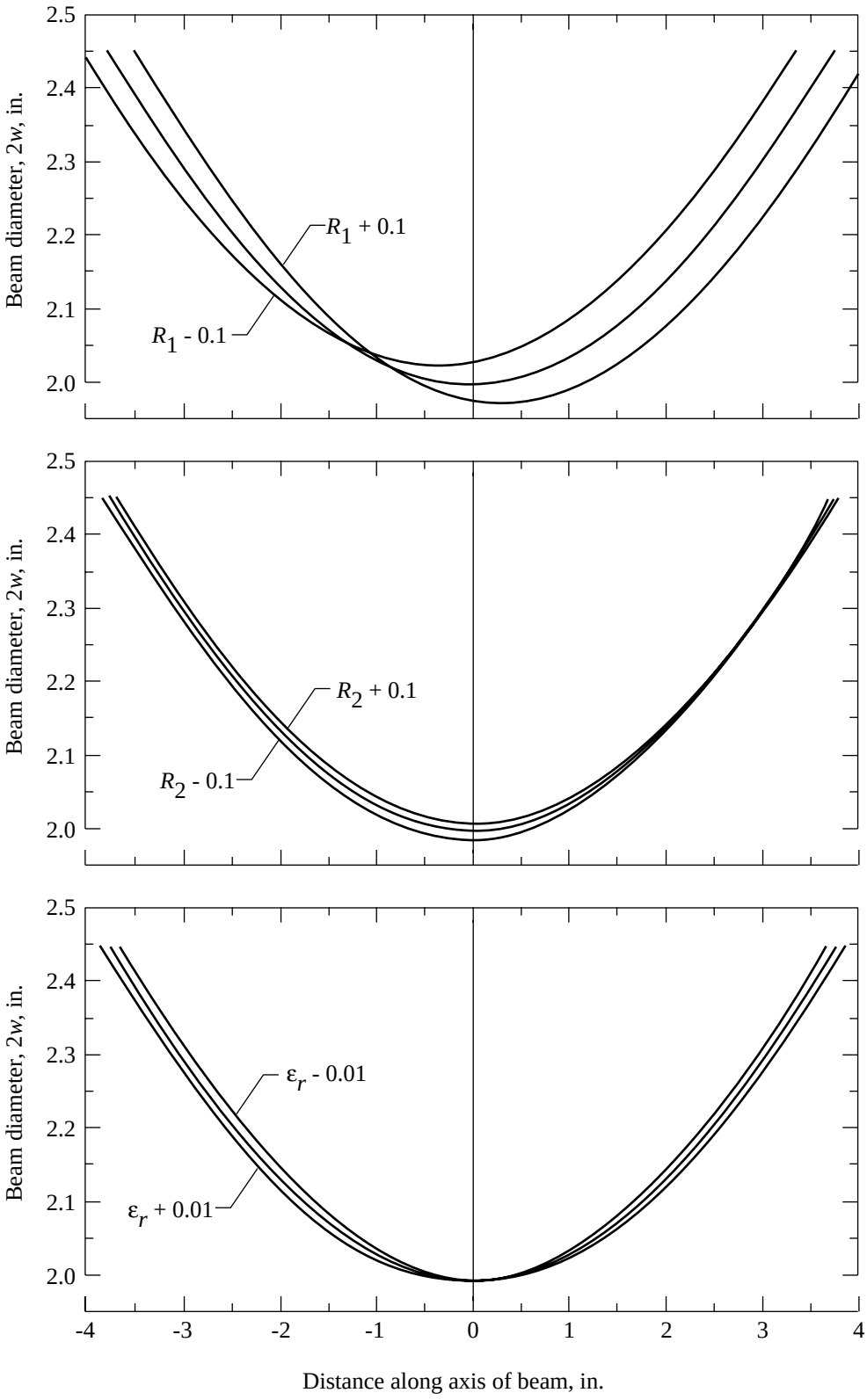

Figure 9. Beam diameter characteristics in test region versus sensitivity to lens errors in 20-GHz beam waveguide system.

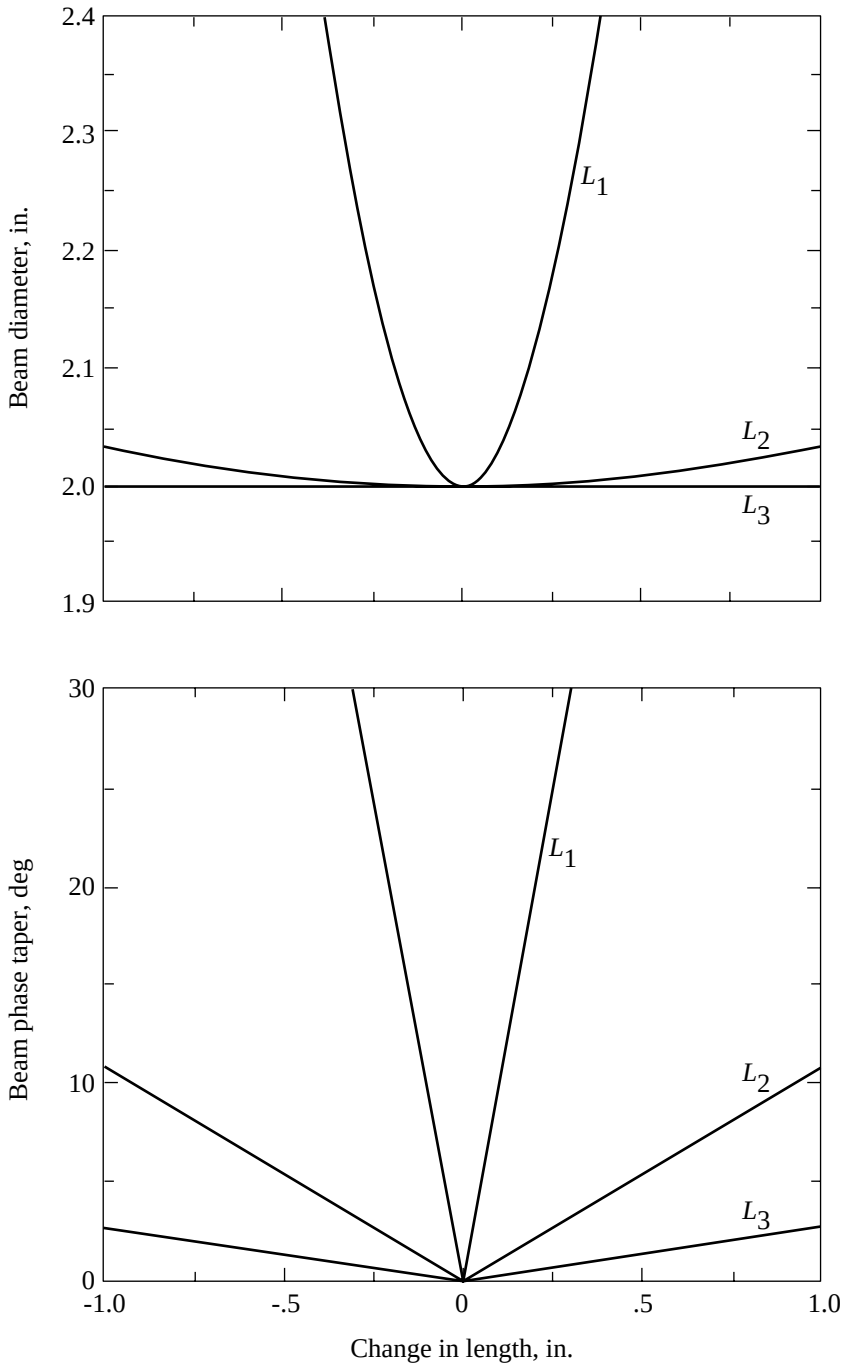

Figure 10. Beam diameter and phase characteristics at center of 20-GHz beam waveguide system versus sensitivity to axial errors.

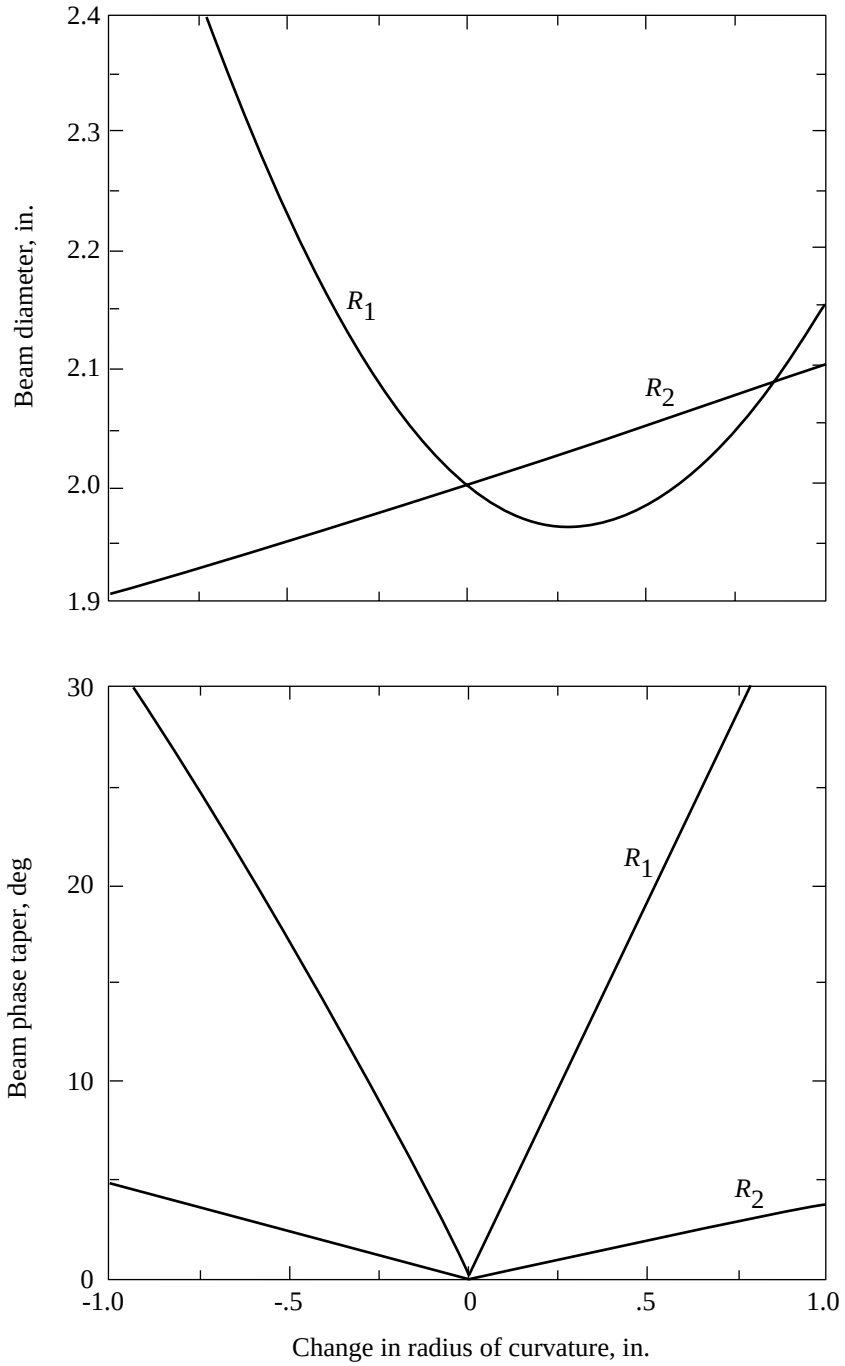

Figure 11. Beam diameter and phase characteristics at center of 20-GHz beam waveguide system versus sensitivity to lens-surface radius of curvature.

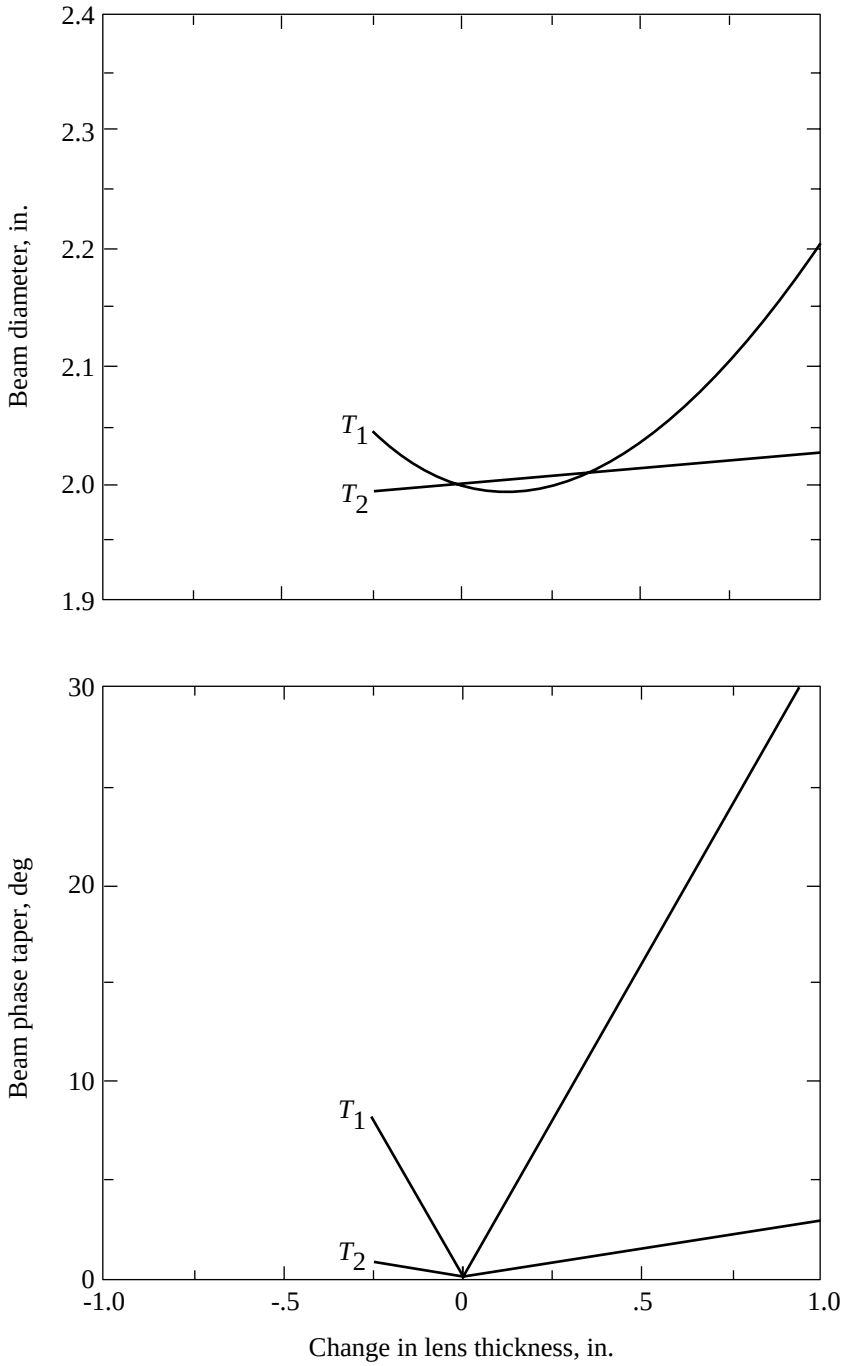

Figure 12. Beam diameter and phase characteristics at center of 20-GHz beam waveguide system versus sensitivity to lens-edge thickness.

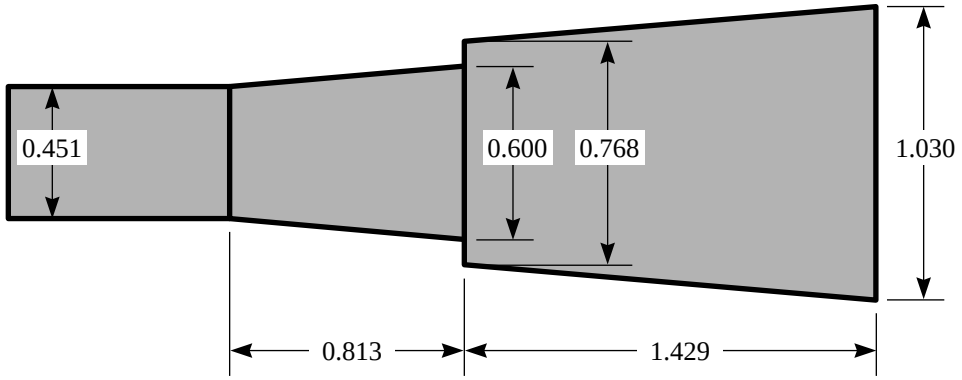

Figure 13. Design dimensions for 20-GHz dual-mode conical horn. All dimensions are given in inches.

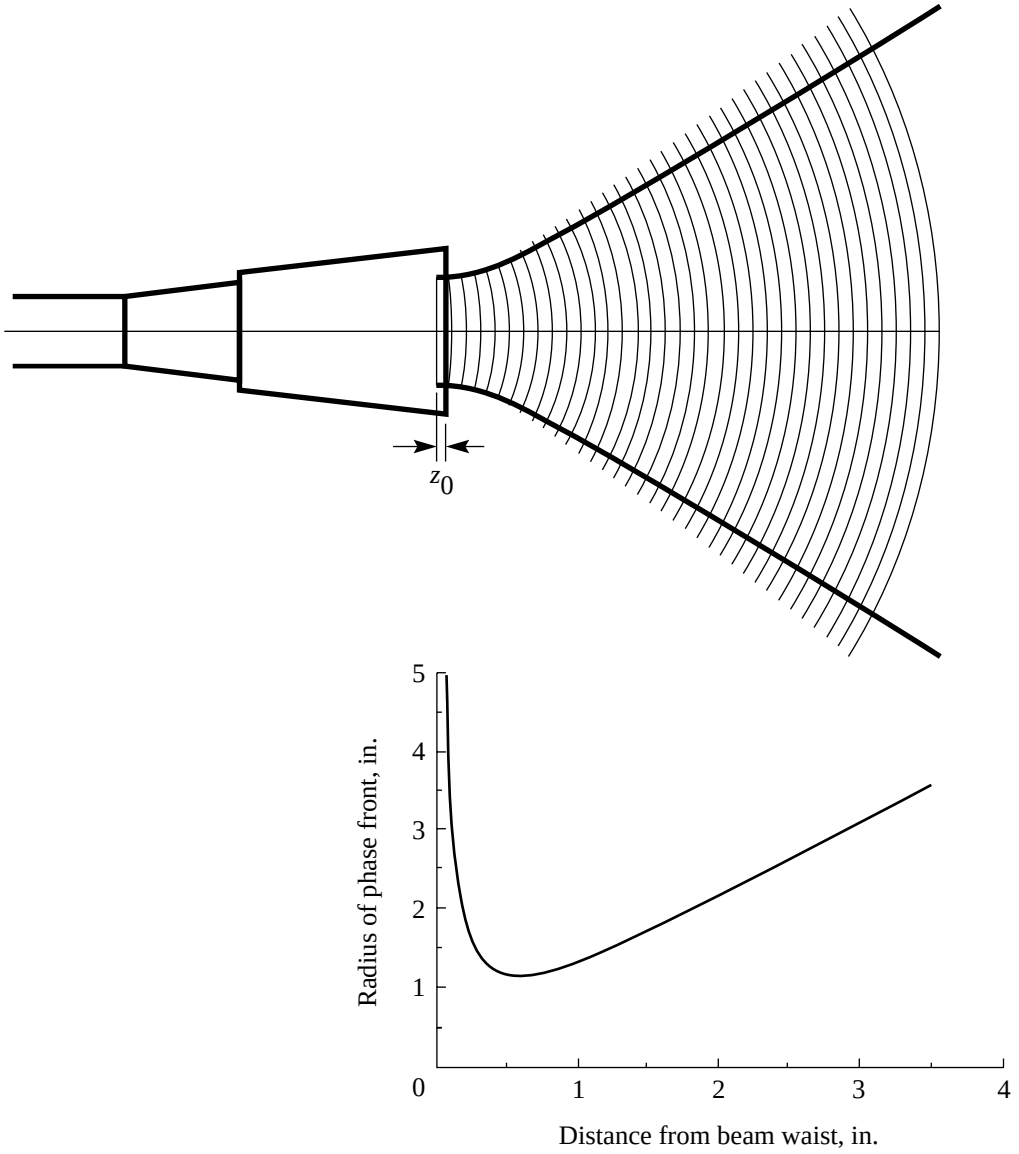

Figure 14. Gaussian beam launched from conical dual-mode horn.

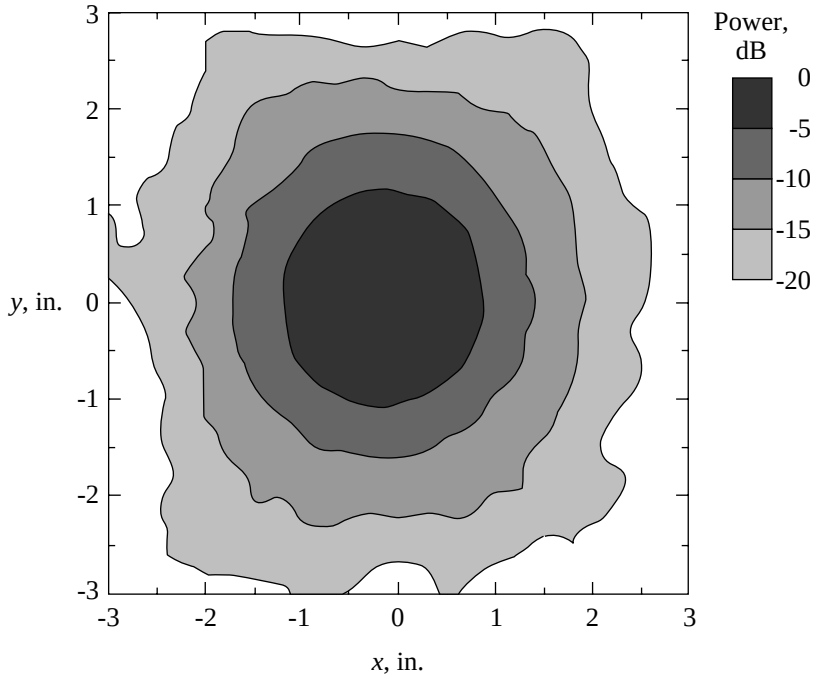

Figure 15. Contour plot of measured amplitude transverse to beam axis at center of 20-GHz beam waveguide system before adjustment of spacing between horn and lens.

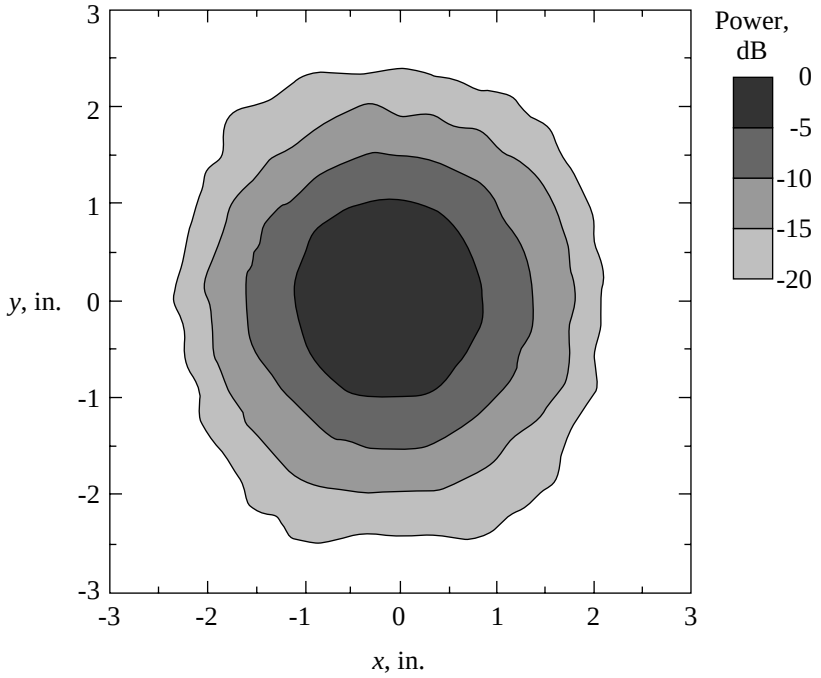

Figure 16. Contour plot of measured amplitude transverse to beam axis at center of 20-GHz beam waveguide system after adjustment of spacing between horn and lens.

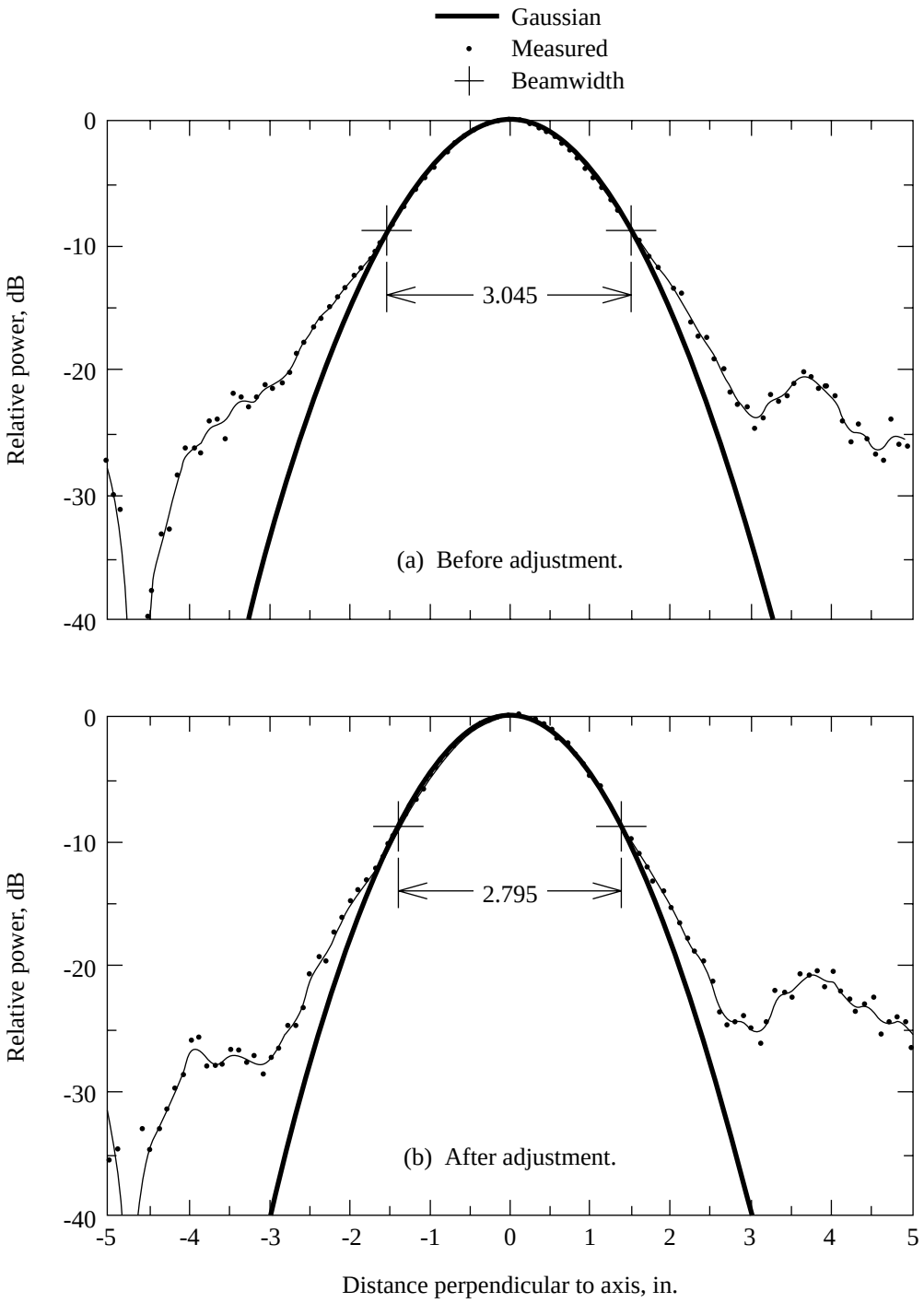

Figure 17. Measured amplitude in H-plane transverse to beam axis at center of 20-GHz beam waveguide system.

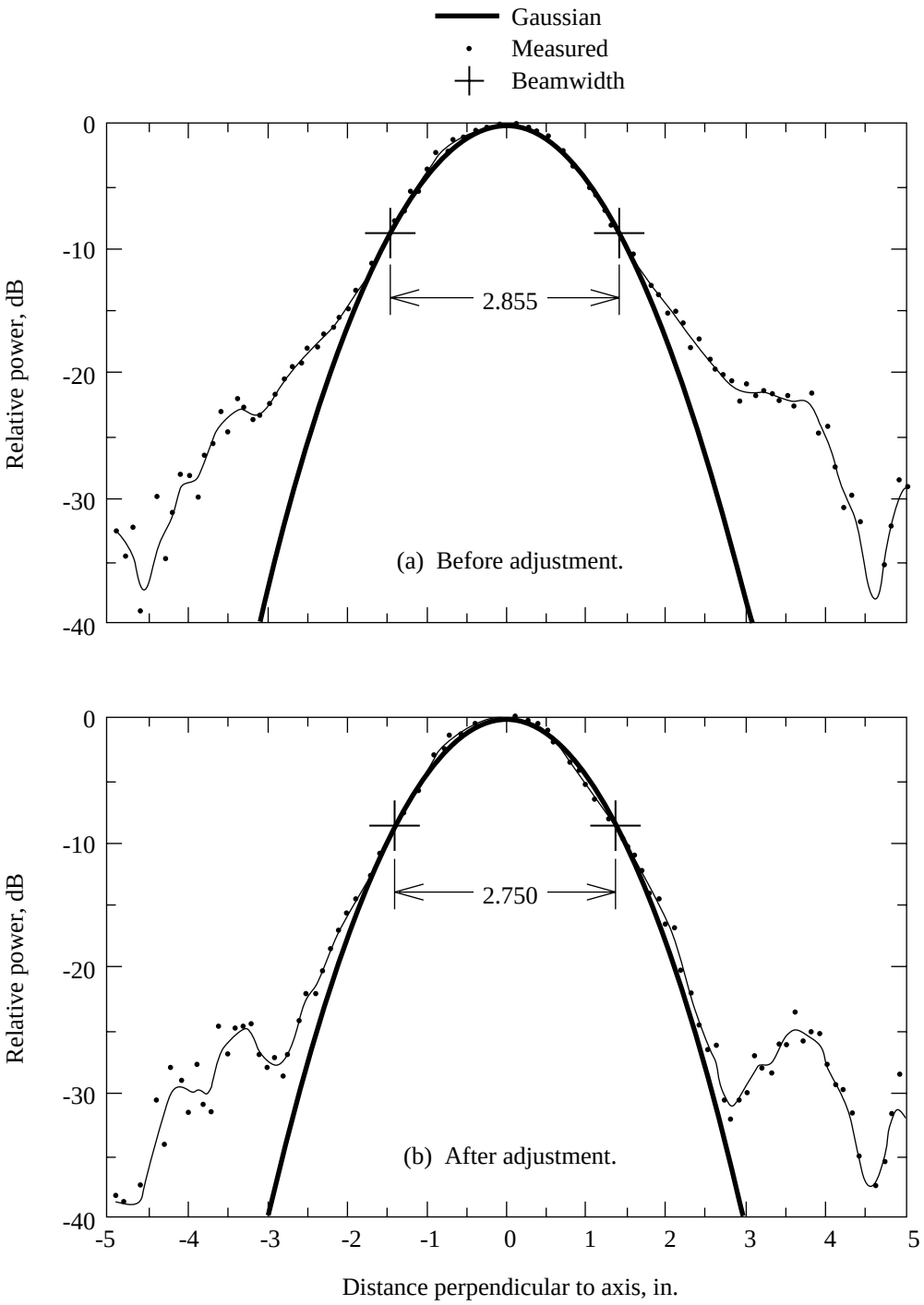

Figure 18. Measured amplitude in E-plane transverse to beam axis at center of 20-GHz beam waveguide system.

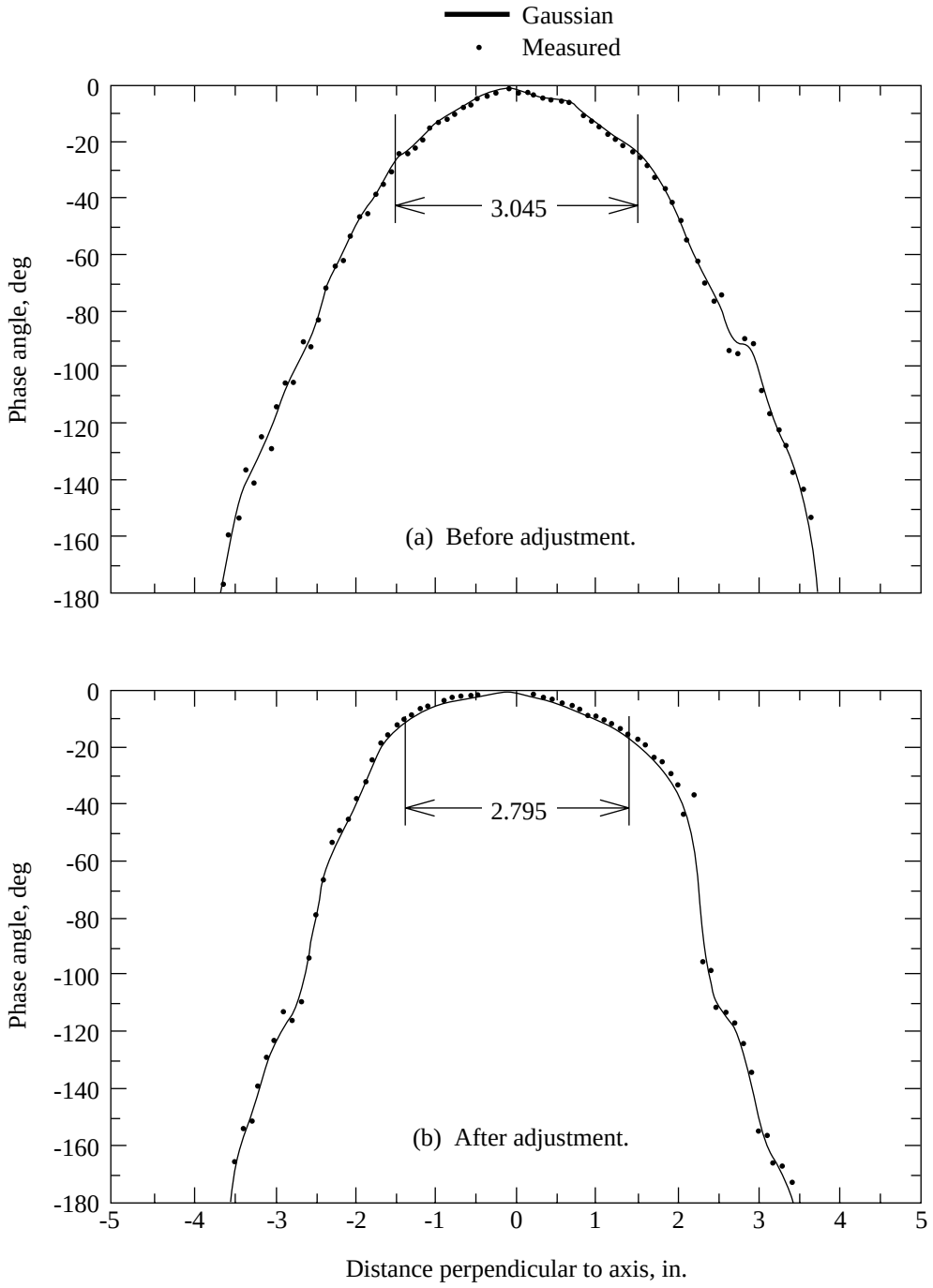

Figure 19. Measured phase in H-plane transverse to beam axis at center of 20-GHz beam waveguide system.

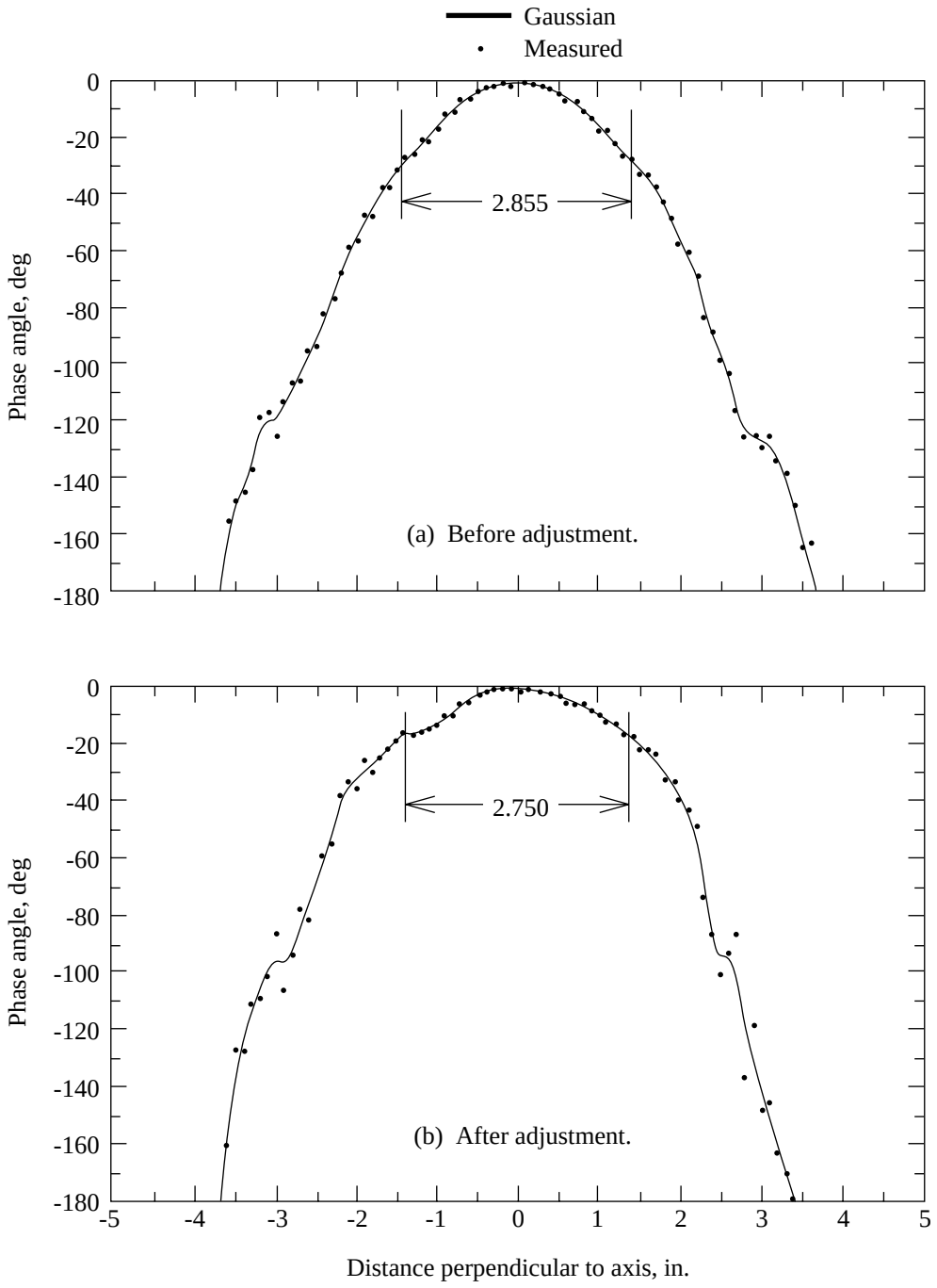

Figure 20. Measured phase in E-plane transverse to beam axis at center of 20-GHz beam waveguide system.

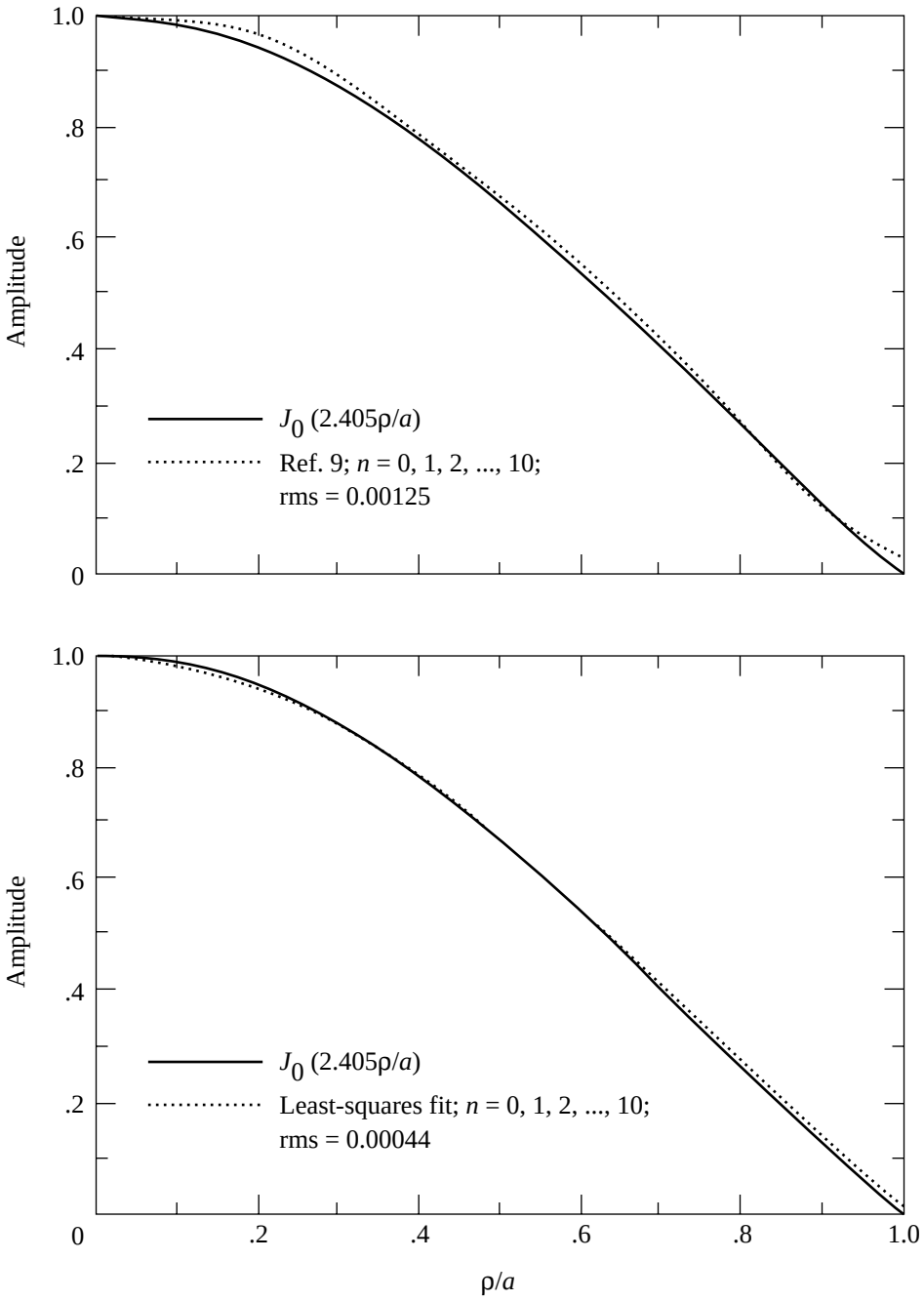

Figure 21. Comparison between Gaussian-Laguerre approximations to aperture field of conical corrugated horn.

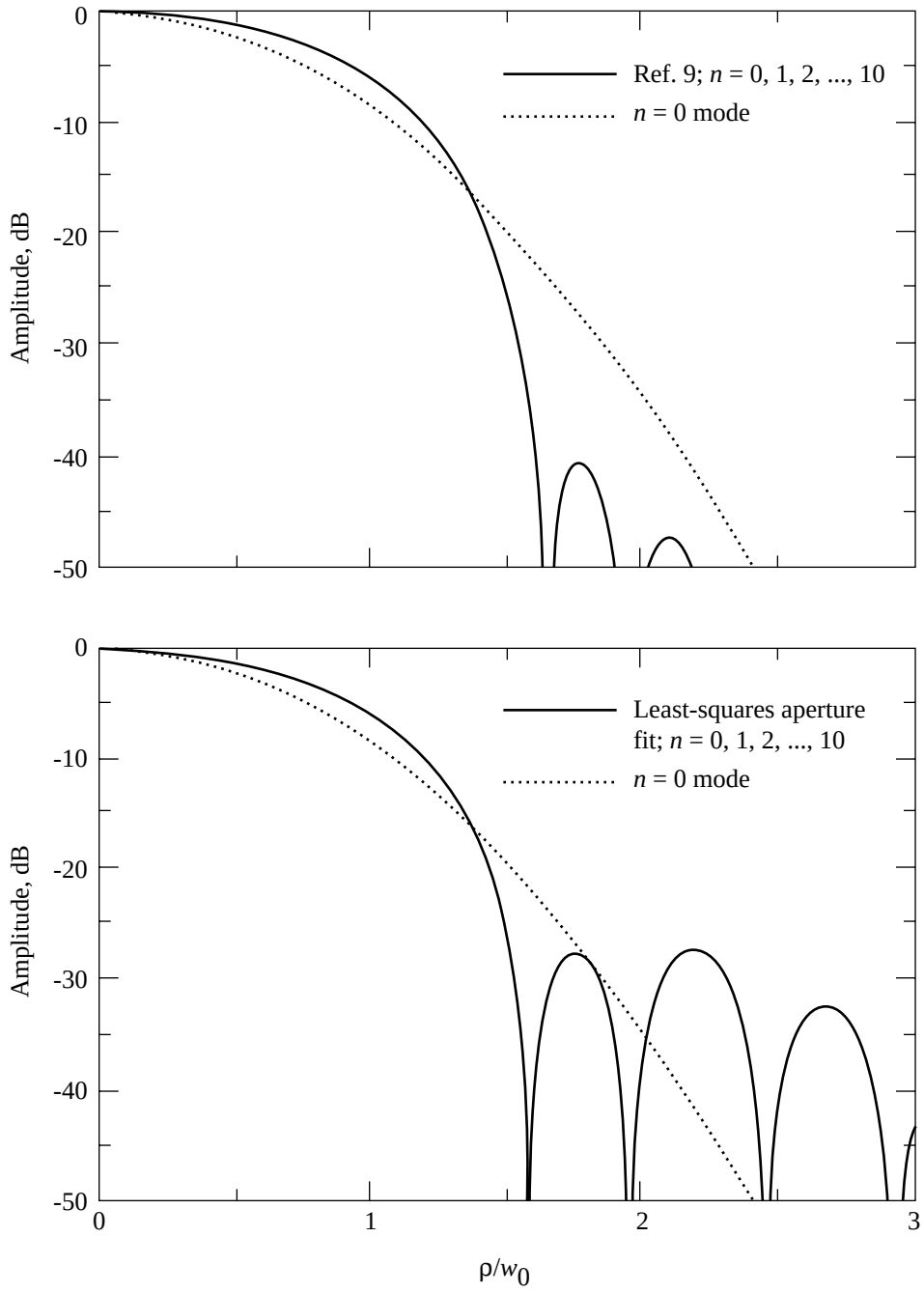

Figure 22. Gaussian-Laguerre approximations of transverse amplitude distribution at center of 20-GHz beam waveguide system.

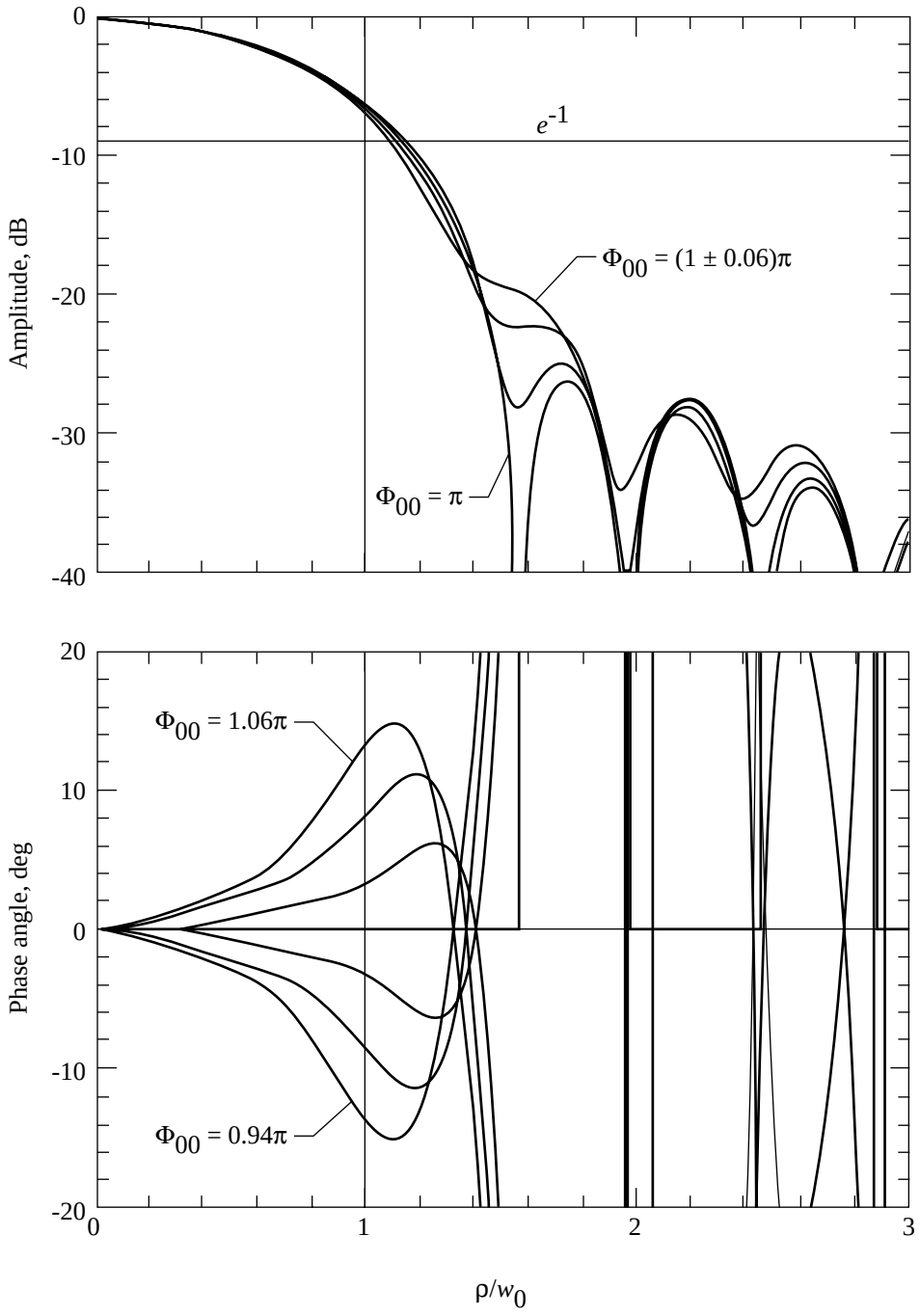

Figure 23. Gaussian-Laguerre approximations of amplitude and phase distribution at center of 20-GHz beam waveguide system versus modal phase slippage.

REPORT DOCUMENTATION PAGE

Form Approved
OMB No. 0704-0188

1. AGENCY USE ONLY *(Leave blank)*	2. REPORT DATE	3. REPORT TYPE AND DATES COVERED
	February 1994	Technical Paper

4. TITLE AND SUBTITLE
Design and Evaluation of an Electromagnetic Beam Waveguide for Measuring Electrical Properties of Materials

5. FUNDING NUMBERS
WU 505-64-52-04

6. AUTHOR(S)
M. C. Bailey

7. PERFORMING ORGANIZATION NAME(S) AND ADDRESS(ES)
NASA Langley Research Center
Hampton, VA 23681-0001

8. PERFORMING ORGANIZATION REPORT NUMBER
L-17298

9. SPONSORING/MONITORING AGENCY NAME(S) AND ADDRESS(ES)
National Aeronautics and Space Administration
Washington, DC 20546-0001

10. SPONSORING/MONITORING AGENCY REPORT NUMBER
NASA TP-3418

11. SUPPLEMENTARY NOTES

12a. DISTRIBUTION/AVAILABILITY STATEMENT
Unclassified–Unlimited

Subject Category 32

12b. DISTRIBUTION CODE

13. ABSTRACT *(Maximum 200 words)*

A beam waveguide has been designed that is based upon the propagation characteristics of the fundamental Gaussian beam and the focusing properties of spherical dielectric lenses. The 20-GHz, two-horn, four-lens system was constructed and experimentally evaluated by probing the field in a plane perpendicular to the beam axis at the center of the beam waveguide system. The critical parameters were determined by numerical sensitivity studies, and the lens-horn critical spacing was adjusted to better focus the beam at the probe plane. The measured performance was analyzed by consideration of higher order Gaussian-Laguerre beam modes. The beam waveguide system was successfully used in the measurements of the electromagnetic transmission properties of Shuttle thermal-protection tiles while the tile surface was being heated to reentry-level temperatures with a high-power laser.

14. SUBJECT TERMS	15. NUMBER OF PAGES
Electromagnetic; Gaussian beam; Waveguide; Lens; Wave propagation; Antennas; Focused fields; Focused beams	31
	16. PRICE CODE A03

17. SECURITY CLASSIFICATION OF REPORT	18. SECURITY CLASSIFICATION OF THIS PAGE	19. SECURITY CLASSIFICATION OF ABSTRACT	20. LIMITATION OF ABSTRACT
Unclassified	Unclassified		